Journal of Nanoscience and Technology 2(3) (2016) 181–185

ISSN: 2455-0191

Contents List available at JACS Directory

Journal of Nanoscience and Technology

journal homepage: www.jacsdirectory.com/jnst

Ammonia Sensing Performance of Nanostructure Cr Doped ZrO_2 Thin Film Deposited by Spray Route

R.H. Bari[1,*], S.B. Patil[1], S.B. Deshmukh[2]

[1]*Nanomaterials Research Laboratory, Department of Physics, G.D.M. Arts, K.R.N. Com. and M.D. Science College, Jamner - 424 206, Maharastra, India.*
[2]*Department of Physics, M.S.G. College, Malegaon – 423 105, Maharastra, India.*

ARTICLE DETAILS

Article history:
Received 27 June 2016
Accepted 06 August 2016
Available online 28 October 2016

Keywords:
Nanostructure
Spray Pyrolysis
Ammonia Gas
Sensitivity

ABSTRACT

Nanostructured thin films of pure ZrO_2 and Cr doped ZrO_2 have been prepared on glass substrate at 350 °C using spray pyrolysis technique. The films were deposited by spraying the solution of CrO_3 and $ZrOCl_2.8H_2O$ having same concentration (0.05 M) in deionized water. Chromic oxide and Zirconium oxychloride were mixed at various volume ratios such as 3:97 %, 5:95 %, 7:93 % and 9:91 %. The films were annealed in air at 550 °C for an hour. These thin films were characterized by XRD, FE-SEM, TEM, SAED pattern and UV spectroscopy technique. The various gases were exposed on films in ambient air at different operating temperature. The Cr doped ZrO_2 thin films showed maximum gas response to ammonia (S=96) for 500 ppm at 300 °C. The parameters like grain size, gas response, selectivity, detection limit, stability, response and recovery time were reported and discussed.

1. Introduction

Nanomaterials are materials which are characterized by an ultrafine grain size (< 50 nm) or by a dimensionality limited to 50 nm. There are many different ways of creating nanostructures. One of them is spray pyrolysis techniques. There are two options, one is direct preparation of nanostructure powder and then it can be utilized for application, second one is synthesis or deposition of thin films [1-4].

Zirconium dioxide is a potential material with large band gap (Eg > 4 eV), high refractive index, high mechanical strength and hardness, fracture toughness, wear and erosion resistance, chemical durability, low thermal conductivity and corrosion barrier properties and have a reasonable barrier height (2 eV) *n*-type semiconductors. It has three crystalline phases, that is, monoclinic (below 1170 °C), tetragonal (1170 to 2370 °C) and cubic (above 2370 °C). Zirconium oxide is doped to stabilize and exhibits abundant oxygen vacancies on its surface. In this work aqueous CrO_3 is used as doping solution. The Cr_2O_3 is P-type semiconductor and forms intergrain metal contacts at boundaries [5, 6].

In the present work, inexpensive spray pyrolysis technique has been used. We have preferred the precursor $ZrOCl_2.8H_2O$ and dopant CrO_3 material for thin film preparation. The prepared thin films were used to test target gases such as H_2, CO_2, CO, NO, NO_2, CH_4, H_2S, SO_2, O_2, NH_3, C_2H_5OH, LPG etc., [7-10].

In the present investigations, we have prepared pure ZrO_2 and Cr doped ZrO_2 thin films by using spray pyrolysis technique. Structural properties, surface morphology, microstructure property, elemental composition and band gap energy were studied using X-ray diffraction (XRD), FE-SEM (Field effect scanning electron microscope), TEM (Transmission electron microscope) and EDAX (Energy dispersive of X-rays) and UV spectroscopy technique respectively. These nanostructured pure ZrO_2 and Cr doped ZrO_2 thin films were tested for different gases.

2. Experimental Methods

2.1 Preparation of Nanostructured ZrO_2 of Thin Films

As prepared precursor solution of $ZrOCl_2.8H_2O$ (0.05 M) was sprayed, through a glass nozzle of 0.1 mm bore diameter on hot glass substrate at temperature 350 °C ± 5 °C at spray rate 5 mL/min for spray deposition time 20 min and these deposited sample was referred as C1. The horizontal movement was kept uniform and compressor air pressure controlled between 3 to 8 kg/cm², this had been done to optimized viscosity and surface tension and momentum of the droplet. Also substrate to nozzle distance played better role. The optimized spray parameters are tabulated in Table 1.

Table 1 Process parameters for the nanostructured pure ZrO_2 and Cr doped ZrO_2 thin films

Spray parameters	Optimum Values
Nozzle	Glass
Nozzle to substrate distance	28 cm
Precursor Solution : Zirconium oxychloride octohydrate solution concentration ($ZrOCl_2.8H_2O$)	0.05 M
Doping Solution: CrO_3	0.05 M
Percentage Variation of dopant solution with base solution	3-97 %, 5-95 %,7-93 % and 9-91 %
Solvent	deionized water
Carrier gas	Compressed air
Substrate temperature	350 °C
Spray deposition time	20 Min
Solution Spray flow	5 mL/min
Carrier pressure	5 kg/cm²

2.2 Preparation of Nanostructured Cr Doped Zro₂ of Thin Films

The glass substrate was cleaned by an ultrasonic cleaner to make surface hydrophilic. As prepared mixture of precursor solution of $ZrOCl_2.8H_2O$ (0.05 M) and doping solution of CrO_3 (0.05 M) in mentioned percentage variation was sprayed through a glass nozzle of 0.1 mm bore diameter, on heated glass substrate at 350 °C±10 °C temperature with constant flow spray rate 5 mL/min by means of air as a carrier gas. The process parameters of spray deposition of Cr doped ZrO_2 thin film is shown in Table 1. The pure ZrO_2 and Cr doped ZrO_2 thin film samples (C1 to C5) were annealed at 550 °C for 1 hour [11-15].

*Corresponding Author
Email Address: rameshbari24@yahoo.com (R.H. Bari)

Cite this Article as: R.H. Bari, S.B. Patil, S.B. Deshmukh, Ammonia sensing performance of nanostructure Cr doped ZrO_2 thin film deposited by spray route, J. Nanosci. Tech. 2(3) (2016) 181–185.

3. Results and Discussion

3.1 Determination of Film Thickness

The film thickness was measured by a weight difference method [12] using relation:

$$t = M/A \cdot \rho \quad (1)$$

where, M is the weight of the sample in g; A the area of the sample in cm^2
ρ the materials density in gcm^{-3}

The thickness of the films was represented in Table 3.

3.2 Structural Properties (X-Ray Diffraction Studies)

As prepared films were characterized by X-ray diffractometer (Philips PW 1730) using Cu Kα radiation (λ = 1.5418 Å). Fig. 1(a-e) shows the XRD pattern of pure ZrO_2 and Cr doped ZrO_2 thin films samples C1, C2, C3, C4 and C5 within range 20 to 80°. X-ray diffractogram of the material was confirmed the polycrystalline and nanocrystalline structures of the ZrO_2. The diffraction peaks from various planes are matching well with standard JCPDS data card for ZrO_2 [16]. The average crystallite size of the pure ZrO_2 and Cr doped ZrO_2 thin film samples were calculated by using the Scherrer's equation and represented in Table 3.

$$D = 0{\cdot}9\lambda/\beta\cos\theta \quad (2)$$

where, D = Average crystallite size; λ = X-ray wavelength (1·5418 Å)
β = FWHM of the peak; θ = Diffraction peak position.

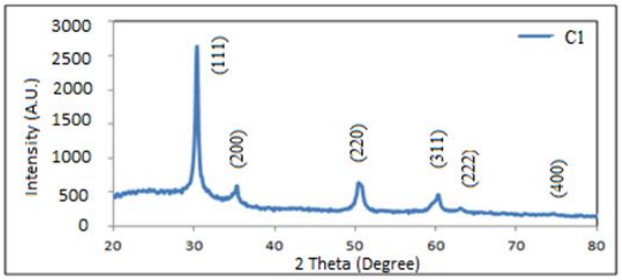

(a)

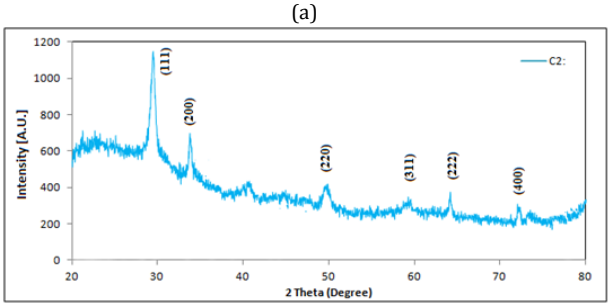

(b)

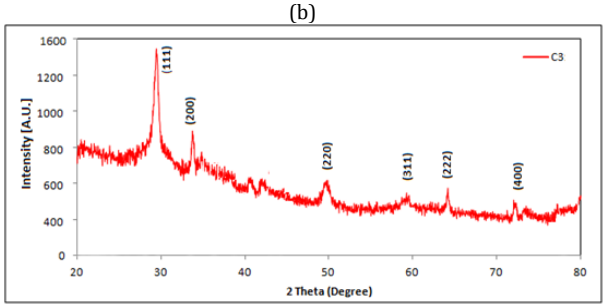

(c)

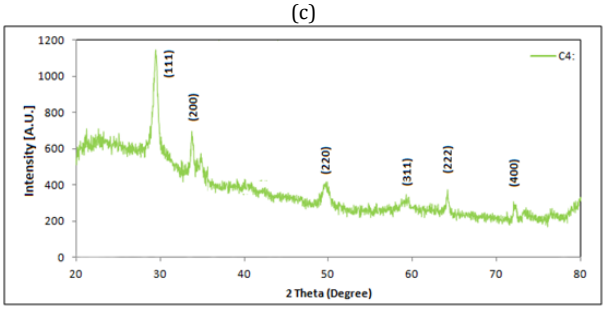

(d)

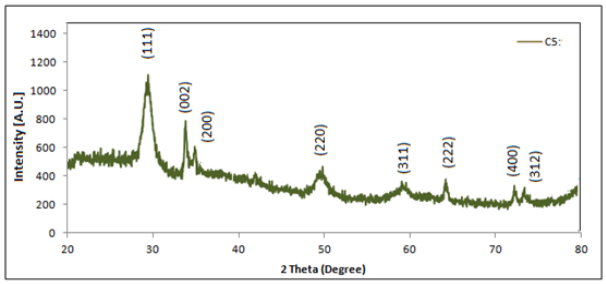

(e)

Fig. 1 (a-e) XRD pattern of the pure ZrO_2 and Cr doped ZrO_2 thin film sample C1 to C5

3.3 Surface Morphology: FE-SEM Analysis

Fig. 2 (C1-C5) depicts the FE-SEM images of pure ZrO_2 and Cr modified ZrO_2 thin films. From these surface morphology observation, it is clear that the structure of the film is nanocrystalline. The uniform film with small spherical grains were developed. The surface morphology of this modified is different than the other dopant. The Cr doped ZrO_2 thin films consists of very small spherical grains grown may be beneficial to gas sensing. Average grain size of the all the film samples (C2-C5) were observed within range 12-15 nm.

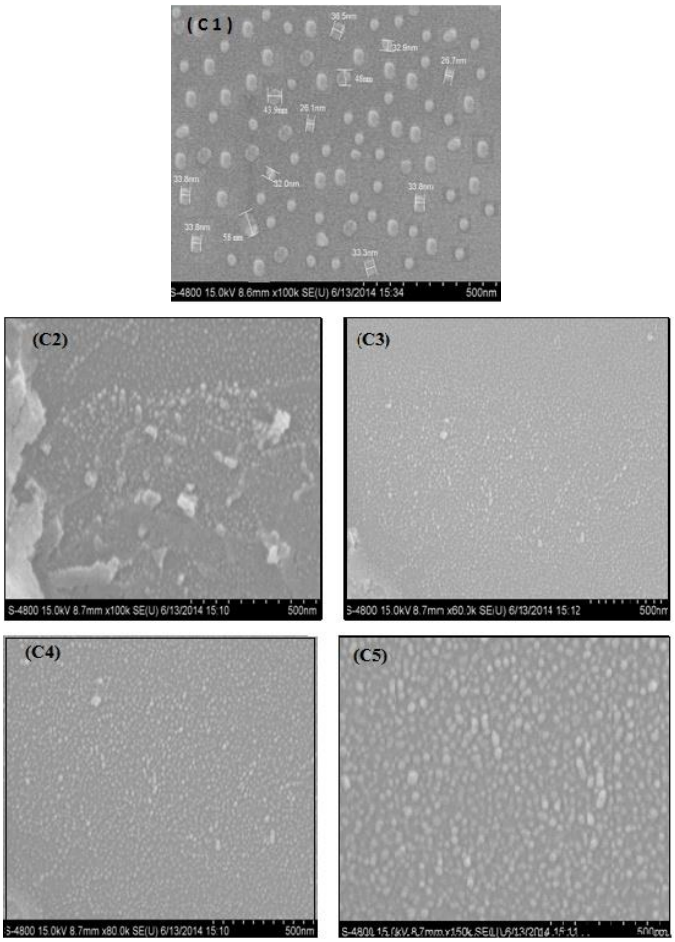

Fig. 2 (C1-C5) FE-SEM images of the nanostructured pure ZrO_2 and Cr doped ZrO_2 thin film samples

3.4 Micro Structural Analysis: TEM Images and SAED Pattern

Fig. 3(a-b) shows the TEM micrograph and SAED pattern of Cr doped ZrO_2 thin film. The surface morphology of the Cr doped ZrO_2 grains observed to be the same by both FE-SEM and TEM micrograph, grains are nanocrystalline and uniform resides over ZrO_2 grains providing with uniform sensing layer. The d values calculated using XRD and SAED pattern for most sensitive sample C3 are tabulated in Table 2. It is well matched with standard JCPDS data card of ZrO_2 [16].

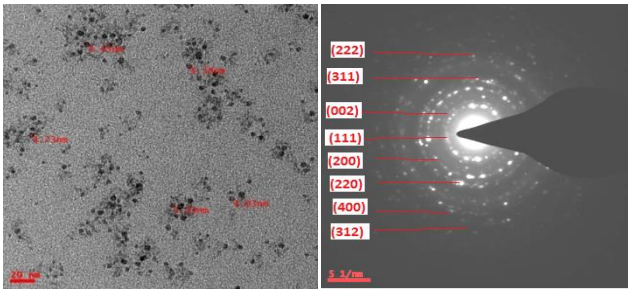

(a) (b)

Fig. 3(a-b) TEM images and SAED pattern of the nanostructured Cr doped ZrO_2 thin film (most sensitive sample =C3)

Table 2 d values for the Cr doped ZrO_2 thin film (most sensitive sample =C3)

(hkl) planes	Reported *d* values (Å)	X-ray diffraction (XRD) *d* values Sample (S1) (Å)	Electron diffraction (TEM) Reciprocal of d values δhkl (nm^{-1})	d values δhkl (nm)
(111)	2.96	2.932	3.381	0.2958
(200)	2.54	2.558	3.912	0.2560
(220)	1.81	1.812	5.494	0.182
(311)	1.54	1.536	6.494	0.154
(222)	1.49	1.474	6.757	0.148
(400)	1.28	1.272	7.813	0.128

Table 3 Size parameters of the pure ZrO_2 and Cr doped ZrO_2 thin film samples

Measuring techniques	Observation	C1	C2	C3	C4	C5
XRD	Crystallite size	4.2 nm	4.8 nm	5.4 nm	5.8 nm	8.2 nm
FE-SEM	Average grain size	12 nm	13 nm	14 nm	16 nm	18 nm
TEM	Average particle size		--	5.9 nm	--	--
SAED	d spacing(111)		--	2.961 Å	--	--
Weight difference	Film thickness		150 nm	230 nm	262 nm	280 nm

From Table 3 it was concluded that as thickness of the films increases, average crystallite size and grain size goes on increases.

3.5 Elemental Compositional Analysis

The quantitative elemental compositions Zr, O and Cr of the pure and doped thin films were tabulated in Table 4. The weight percentage of Cr is different for each with oxygen deficiency. The deficiency of oxygen reduces the resistance of the film and would promote the adsorption of oxygen species favorable for higher gas response at increase in temperature.

Table 4 Elemental compotitional analysis of Cr_2O_3 modified ZrO_2 thick films

Element	Sample C1		Sample C2		Sample C3		Sample C4		Sample C5	
	mass %	at %	mass %	at %	mass %	at %	mass %	at %	mass %	at %
O	23.42	63.6	11.53	42.23	67.34	73.06	29.44	70.23	69.48	46.25
Zr	76.55	36.4	86.48	55.54	37.04	26.69	69.77	29.19	26.31	51.48
Cr	-	-	1.98	2.24	0.58	0.25	0.29	0.58	4.21	2.27
Total	100	100	100	100	100	100	100	100	100	100

Pure ZrO_2 thin film sample (C1) was observed to be nonstoichiometric in nature. It is clear from Table 4 that at % of Cr goes on increasing with increasing wt % of Cr in ZrO_2 thin films (C2-C5).

3.6 Optical Properties : Absorption Spectra

Optical absorption spectra (Fig. 4) carried out using JASCO UV-VIS-NIR Model V-670 Spectrophotometer. Fig. 4 represents the absorption spectra of pure ZrO_2 and Cr doped ZrO_2. After modification, absorption spectra tremendously changed. It is flat above 500 nm wavelength and the absorption increases between 300 to 460 nm and thereafter it was observed to be decreased [10-15]. The band gap energies of the samples were calculated from the absorption edges of the spectra. The slope drawn from the start of an absorption edge (the onset of absorbance) and horizontal tangent had drawn on absorption minimum and intercepted each other at some point. The vertical line drawn from this point on wavelength axis gave the absorption edge wavelength [16].

The bang gap energy for the pure ZrO_2 found to be 4.46 eV and Cr doped ZrO_2 thin films were in the range of 2.4 to 2.8 eV. Large change in optical band gap energy due to the change in grain size and formation of nonocrystalline nature of the thin films.

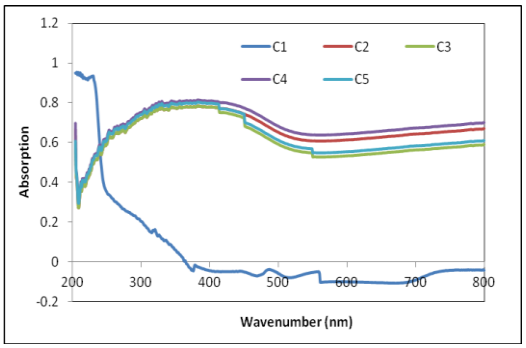

Fig. 4 Absorption spectra of pure ZrO_2 and Cr doped ZrO_2 thin samples

3.7 Electrical Characterization

3.7..1 I-V Characteristics

Fig. 5 shows the I-V characteristics of pure ZrO_2 and Cr doped ZrO_2 thin film samples, it shows the semiconducting nature and good ohmic contact.

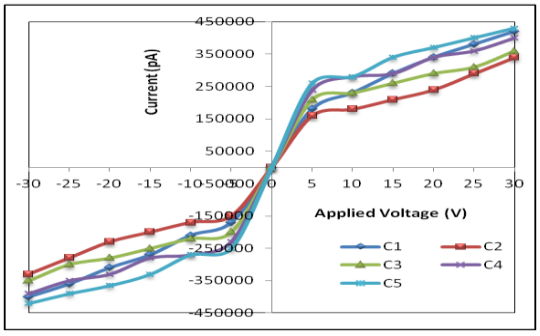

Fig. 5 I-V chracteristics of the pure ZrO_2 and Cr doped ZrO_2 thin film samples

3.7.2 Conductivity Profile

The conductivity of the film samples C1 to C5 is shown in Fig. 6. The increase in conductivity of the sensor with an increase in temperature could be attributed to the semiconducting nature and negative temperature coefficient of the sensor resistance.

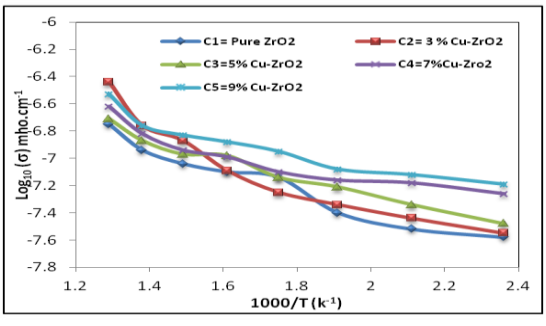

Fig. 6 Conductivity profile of pure ZrO_2 and Cr doped ZrO_2 thin films

3.8 Gas Sensing Performance of Thin Films

3.8.1 Gas response

The gas response determined using the formula,

$$S = Gg\text{-}Ga/Ga \quad (3)$$

where, Ga = the conductance of the sensor in air
Gg = the conductance on exposure of a target gas

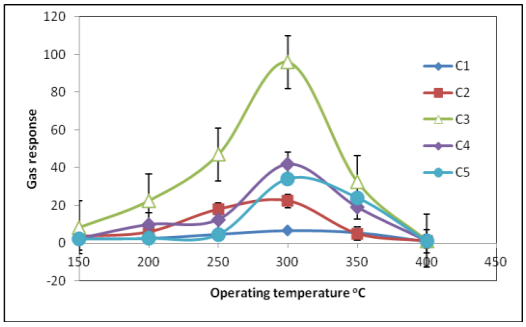

Fig. 7 Variation of NH_3 gas with respect to operating temperature

The gas response of NH_3 to sample C1,C2,C3,C4 and C5 have been tested at different operating temperature is shown in Fig. 7. All the samples shown response to ammonia.The maximum gas response was obtained to sample C3 (S=96) at 300 °C for 500 ppm. It is well-known that the response of the metal–oxide semiconductor sensors is mainly determined by the interactions between a target gas and the surface of the sensor [17, 18].

3.8.2 Selectivity

Selectivity of pure ZrO_2 and Cr doped ZrO_2 thin films were measured at an operating temperature of 300 °C. Fig. 8 depicts the bar diagram to indicate NH_3 selective ability of the sensor.

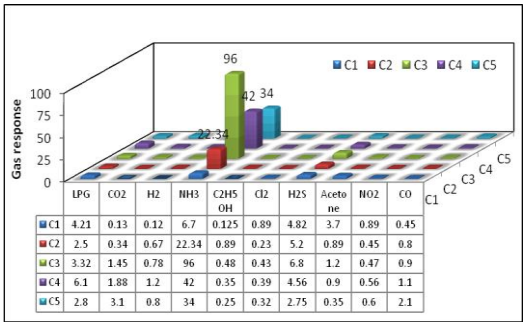

	LPG	CO2	H2	NH3	C2H5 OH	Cl2	H2S	Aceto ne	NO2	CO
C1	4.21	0.13	0.12	6.7	0.125	0.89	4.82	3.7	0.89	0.45
C2	2.5	0.34	0.67	22.34	0.89	0.23	5.2	0.89	0.45	0.8
C3	3.32	1.45	0.78	96	0.48	0.43	6.8	1.2	0.47	0.9
C4	6.1	1.88	1.2	42	0.35	0.39	4.56	0.9	0.56	1.1
C5	2.8	3.1	0.8	34	0.25	0.32	2.75	0.35	0.6	2.1

Fig. 8 Selectivity of NH_3 at optimal temperature 300 °C

3.8.3 Calibration Curve and Detection Limit

The variation of NH_3 gas response with respective to gas concentration at operating temperature 300 °C is shown in Fig. 9. The gas response increased in the range 10 to 500 ppm and reached 96 in the presence of 500 ppm of NH_3 gas and there after it is in saturation. The detection limit is to be estimated as 10 ppm.

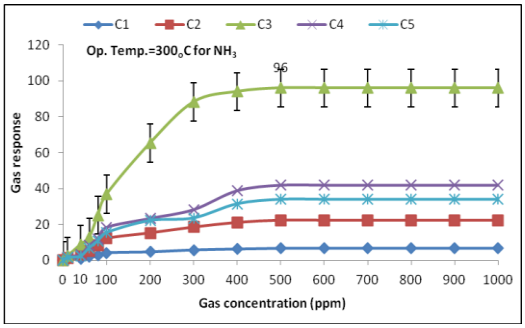

Fig. 9 Variation of NH_3 gas response with concentration (ppm)

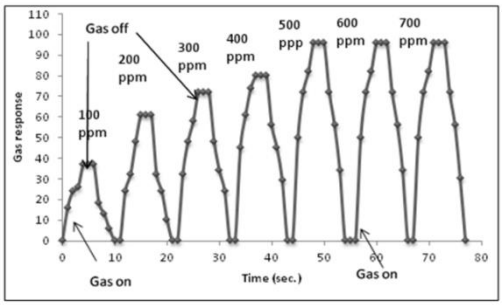

Fig. 10 Respose and recovery time for sample C3 (most sensitive sample)

3.8.4 Response and Recovery Time

Fig. 10 represents the response and recovery profole of the most sensitive sample C3. The response is quick (4 s) and recovery is fast (12 s).

The high oxidizing ability of adsorbed oxygen species on the surface nanoparticles and high volatility of desorbed by-products explain the quick response to H_2S and fast recovery [19-21].

3.8.5 Stability

Fig. 11 shows the stability of pure ZrO_2 and Cr doped ZrO_2 thin films, which were measured by repeating the target gas test many times (cycle one day per week). During the test no significant variation was recorded as shown Fig. 11 Ammonia gas modified thin film sensor had prominent long term stability in atmosphere for around 10 weeks. The obtained change in electrical conductance during repetitive exposure of acetone is stable and reproducible.

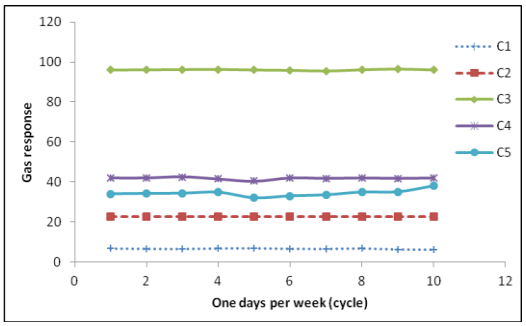

Fig. 11 Stability profile of pure ZrO_2 and Cr doped ZrO_2 thin film samples

3.8.6 Comparison of NH_3 Response of Reported Doped Thin Film Sensors with Sensor Prepared in the Present Paper

Table 5 presents comparison of NH_3 response with reported different sensor and sensor prepared in present investigation [17-20]. It is clear that response of sensor reported in the present work is extremely high as compared to previous reported sensors.

Table 5 Comparison of NH_3 response with previous reported work

Form of material/ sensor	Gas Response	Gas conc. (ppm)	Gas response/ Sensitivity	Operating Temperature (°C)	Reference
Cr-ZrO_2 (SP-Thin film)	NH_3	500	96	300	Present work
Ni-ZnO (Spin-Thin film)	NH_3	1000	9.5	190	17
Ni_2O_3-WO_3 (Sputter-Thin)	NH_3	200	13.5	250	18
Cu-ZnO (SP-Thin film)	NH_3	1000	35	400	19
Ni-ZnO	NH_3	1000	2.52	--	20

The physisroption and chemisorption is very important in case of gas sensing mechnism. The reaction kinetic because of adsorption occurs as a consequence of oxygen species O_2, O_2^-, O^{2-} may be expalined by the reaction [19-21].

Oxygen in air is adsorbed onto material surface,

$$O_{2(gas)} \Leftrightarrow O_{2(ads)} \quad (4)$$

The adsorbed oxygen changes to ions O2- following the reaction

$$O_{2(ads)} + e^- \Leftrightarrow O^-_{2(ads)} \quad (5)$$

At high temperature the ions O2- rapidly changes to ions O-

$$O^-_{2(ads)} + e^- \Leftrightarrow 2O^- \quad (6)$$

Above 150 to 175 °C, the reactivity of O^{2-+} species is high; the formation of O^{2-} species is also possible as follows

$$O^-_{ads} + e^- \Leftrightarrow O^{2-} \quad (7)$$

The schematic of adsorption and desorption on film surface layer is shown in Fig. 12. The gas sensing performance was tested for 500 ppm concentration. The sample had shown maximum response to ammonia

than other gases. The sample C3 had showed (Gas response = 96) than other sample. In this modified sample Cr content are optimum and surface morphology becomes nanostructure with small uniform grains. Reside over base material ZrO_2.The surface to volume ratio have been increased, it results increase in ammonia gas response. The ionic size of chromium is (0.62 Å) is less than (Zr^{+4}) ions, also it is trivalent acceptor impurity p -type oxide forming hetreojunction at grain boundaries. Effect of Cr is expressed by Eq. (8)

$$Cr_2O_3 \xrightarrow{ZrO_2} 2Cr'_{Zr} + V_O^{**} + 3O_O^x \quad (8)$$

where V_o represents oxygen vacanices and Cr_{Zr} means Cr substitution in Zr. It has been oberved that doping with unstable cation provides that hortet route by altering electronic and catalytic properties of ga interaction at interface. Therefore it improves the gas response. The resistance significantly reduced and the reduction in garrier height enhanced gas response [19].

$$2Cr_2S_3 + 9O_2 \rightarrow 2Cr_2O_3 + 6SO_2 \quad (9)$$

Similarly when reducing gas NH_3 comes into contact the grains of Cr doprd ZrO_2 thin film , at elevated temperature ammonia reacts with the film surface and adsorbed oxygen on the surface of the film get oxidized ammonium hydroxide, liberating free electrons in the conduction band,

$$ZrO_2 + 5NH_{3(gas)} + 4O_2^-(\text{filmsurface}) \rightarrow Zr(NH_4OH)_{3(\text{filmsurface})} + 2NO_{2(gas)} + 8e^-(\text{conductionband}) \quad (10)$$

This shows n-type conduction mechanism, thus generated electron contribute to sudden increase in conductance of the thin film, which may be due to surface reaction of ammonia with physisorbed H_2O or by proton conductivity via NH^{4+} cations, Cr_2O_3 may generate the solid acidity on the solid base ZrO_2. The acidity on the sensor surface would form NH^{4+} cations, which constitutes the proton conductivity leading to a crucial decrease of the resistance. This would decrease the barrier height among the Cr_2O_3-ZrO_2 grains.

$$NH_{3(gas)} + H_2O(\text{surface}) \rightarrow NH_4OH_{(gas)} \quad (11)$$

Ammonia hydroxide NH_4OH produced during the surface reaction is volatile in nature. The high volatility of NH_4OH influences the quick response and fast recovery of the thin film sensor [20, 21].

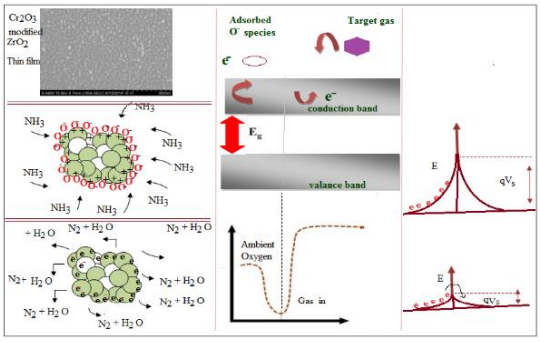

Fig. 12 Schematic of ammonia sensing on Cr doped ZrO_2 thin film

4. Conclusion

Nanostructured pure ZrO_2 and Cr doped ZrO_2 thin films prepared by simple and inexpensive spray pyrolysis technique onto the glass substrates. The average crystallite sizes were observed from XRD and it was found to be 5.8 nm. FESEM analysis revealed that, the grains were spherical in shape with grain size around 14 nm. TEM images showed the particle size ~4.8 nm. EDAX analysis confirmed that the Cr modified ZrO_2 thin film was observed to be oxygen dificience.Optical study reveals that Cr doping increases the optical band gap energy varying from 2.4 to 2.8 eV. Gas response of Cr doped ZrO_2 thin film towards NH_3 gas. Cr doped ZrO_2 thin film helped to enhance the gas response (S=96), and selectivity towards NH_3 gas. Selectivity study showed that films were most selective to NH_3 gas. Speed of response (4 s) and fast recovery (12 s) is main feature of the sensor. The prepared thin films show good stability.

Acknowledgement

Authors are thankful to Principal's of G.D.M. Arts, K.R.N. Commerce and M.D. Science College, Jamner, and MSG Arts, Science and Commerce College, Malegaon. Also thankful to Department of Physics, SPPU, Pune and NMU, Jalgaon to providing necessary laboratories facilities for analytical characterization.

References

[1] H.R. Kim, K. Choia, J.H. Lee, S.A. Akbar, Highly sensitive and ultra-fast responding gas sensors using self-assembled hierarchical SnO_2 sphere, Sens. Actuators B 136 (2009) 138-143.
[2] G. Zhang, M. Liu, Effect of particle size and dopant on properties of SnO_2-based gas sensors, Sens. Actuators B 69 (2000) 144-152.
[3] J.M. Patil, S.B. Patil, R.H. Bari, R.T. Chaudhari, A.N. Sonar, Influence of film thickness on structural, surface morphology and electrical properties of spray pyrolise nanostructured WO_3 thin films, J. Adv. Phys. 5 (2016) 1-5.
[4] R.H. Bari, Gas sensing performance of chemically deposited nanocrystalline Cu_2S thin films, Inter. J. Technol. Chem. Res. 02 (2016) 133-140.
[5] C. Santato, M. Odziemkowski, M. Ulmann, J. Augustynski, Crystallographically oriented mesoporous WO_3 films: Synthesis, characterization, and applications, J. Amer. Chem. Soc. 123 (2001) 10639-10649.
[6] Y.S. Kim, H. Seung-Chul, K. Kim, H. Yang, S.Y. Choi, et al, A systematic review on incidence, severity, outcome and prevention, Appl. Phys. Lett. 86 (2005) 213105-213112.
[7] K. Sayama, K. Mukasa, R. Abe, Y. Abe, H. Arakawa, Stoichiometric water splitting into H_2 and O_2 using a mixture of two different photocatalysts and an IO_3-/I- shuttle redox mediator under visible light irradiation, Chem. Commun. 01 (2001) 2416-2423.
[8] J.L. Solis, Highly porous tungsten-oxide-based films obtained by spray-gel for gas sensing Applications, Rev. Mexicana De Fisica 52 (2006) 29-31.
[9] M. Ferroni, V. Guidi, G. Martinelli, G. Sberveglieri, Microstructural characterization of a titanium-tungsten oxide gas sensor, J. Mater. Res. 12 (1997) 793-798.
[10] V. Srivastava, A.K. Srivastava, K.N. Sood, K. Jain, Sol gel synthesis of tungsten oxide thin film in presence of surfactant for NO_2 detection, J. Sens. Transducers 107 (2009) 99-110.
[11] R.H. Bari, S.B. Patil, Nanostructured spray pyrolysis zinc doped CdO thin films for LPG gas sensor, J. Nanosci. Technol. 2(2) (2016) 104-108.
[12] J.M. Patil, S.B. Patil, R H. Bari, A.N. Sonar, Conventional gas sensor application of nanostructured WO_3 thin films, Sens. Lett. 13 (2015) 1-8.
[13] R.H. Bari, S.B. Patil, A.R. Bari, Influence of precursor concentration solution on CO sensing performance of sprayed nanocrystalline SnO_2 thin films, Optoelect. Adv. Mater. Rapid Commun. 6 (2012) 887-895.
[14] Simon, N. Barson, Micro machined metal oxide gas sensors: opportunities to improve sensor performance, Sens. Actuators B 73 (2001) 1-26.
[15] R.H. Bari, S.B. Patil, Improved NO_2 sensing performance of nanostructured Zn doped SnO_2 thin films, Int. J. Technol. Chem. Res. 01 (2015) 86-96.
[16] JCPDS Data Card (JCPDS 36-020) and (JCPDS 17-0923).
[17] K.C. Sharma, J.C. Garg, Influence of thermal annealing in air on the electro optic characteristic of chemical bath deposited non-stoichiometric cadmium zinc selenide thin films, Phys. D: Appl. Phys. 23 (1990) 1411-1419.
[18] R. Kumar, S.A. Imam, M.R. Khan, A critical review of Taguchi gas sensor for the detection of VOC'S, MASAUM J. Rev. Surv. 1 (2009)177-183.
[19] L.A. Patil, A.R. Bari, M.D. Shinde, Vinita Deo, Ultrasonically prepared nanocrystalline ZnO thin films for highly sensitive LPG sensing, Sens. Actuators B: Chem. 149 (2010) 79-86.
[20] L.A. Patil, A.R. Bari, M.D. Shinde, Vinita Deo, Ultrasonically synthesized nanocrystalline ZnO powder based thick film sensor for ammonia sensing, Sens. Rev. 30 (2010) 290 - 296.
[21] L.A. Patil, A.R. Bari, M.D. Shinde, Vinita Deo, D.P. Amalnerkar, Synthesis of ZnO nanocrystalline powder from ultrasonic atomization technique, characterization, and its application in gas Sensing, IEEE Sens. 11 (2011) 939-946.